## **Soft Matter**



PAPER View Article Online



Cite this: DOI: 10.1039/c9sm02363a

# Inverse leidenfrost drop manipulation using menisci†

Anaïs Gauthier, 10 \* Guillaume Lajoinie, Jacco H. Snoeijer and Devaraj van der Meer

Drops deposited on an evaporating liquid bath can be maintained in an inverse Leidenfrost state by the vapor emanating from the bath, making them levitate and hover without effective friction. These perfectly non-wetting droplets create a depression in the liquid interface that sustains their weight, which generates repellent forces when they approach a meniscus rising against a wall. Here, we study this reflection in detail, and show that frictionless Leidenfrost drops are a simple and efficient tool to probe the shape of an unknown interface. We then use the menisci to control the motion of the otherwise elusive drops. We create waveguides to direct and accelerate them and use parabolic walls to reflect and focus them. This could be particularly beneficial in the scale up of droplet cryopreservation processes: capillary interactions can be used to transport, gather and collect vitrified biological samples in absence of contact and contamination.

Received 1st December 2019, Accepted 31st March 2020

DOI: 10.1039/c9sm02363a

rsc.li/soft-matter-journal

Droplets deposited on a cryogenic liquid, such as liquid nitrogen can be levitated through the action of an insulating vapor layer originating from the bath.<sup>1,2</sup> This phenomenon is called the inverse Leidenfrost effect, by comparison with the usual Leidenfrost situation where volatile liquids are levitated above a hot solid.3-6 In both cases, the levitating particles are extremely mobile,<sup>7,8</sup> and controlling their motion is a challenge.<sup>9</sup> Solid substrates can be sculpted to control drop motion, either macroscopically by giving them a curved shaped 10 (e.g. similarly to the spoon used by J. G. Leidenfrost<sup>3</sup>) or at a smaller scale by using textures to redirect the vapor below the drop. 11,12 Such strategies have not been proposed on liquids, where they are difficult to implement. Nonetheless, liquids can be reshaped up to the millimeter scale, using surface tension forces. In particular, the liquid interface distorts and creates a meniscus in the presence of a wall. For wetting liquids (with a contact angle  $\theta < 90^{\circ}$ ) the liquid rises along solid interfaces over a characteristic distance equal to the capillary length a. Floating objects interact with these menisci, often in an attractive way: small bubbles are seen to drift towards the edge of a glass<sup>13</sup> and particles (colloids, plant seeds) spontaneously climb them<sup>14</sup> and even spontaneously self-assemble. 15,16 On the contrary, hydrophobic objects (with contact angle >90°) such as liquid marbles<sup>17,18</sup> or insects<sup>19–23</sup> are repelled by wetting menisci. Levitating drops, which are perfectly non-wetting also bounce away from (wetting) menisci,<sup>24</sup>

Physics of Fluids group and Max Plank Center Twente, Mesa + Institute and Faculty of Science and Technology, J. M. Burgers Centre for Fluid Dynamics and Max Plank Center Twente for Complex Fluid Dynamics, University of Twente, P. O. Box 217, 7500 AE Enschede, The Netherlands. E-mail: anais.gauthier@espci.fr

† Electronic supplementary information (ESI) available. See DOI: 10.1039/c9sm02363a

which has successfully been used to confine Leidenfrost droplets to a specific location.<sup>9</sup>

In this paper, we propose to use the repellency of inverse Leidenfrost droplets by menisci as a way to finely tune and control drop motion. To this end, we first model the droplet interaction with a single wall and subsequently combine multiple structures to enforce particle motion in a controlled direction, accelerate them and focus them onto a chosen location. Our systems might be useful in droplet cryopreservation processes, where droplets containing biological materials are vitrified on a liquid nitrogen bath. We demonstrate here that capillarity can be used to efficiently transport and collect multiple samples in absence of any contact and thus avoiding contamination.

## 1 Experiment

Millimeter-sized silicone oil droplets (density  $\rho=930~{\rm kg~m}^{-3}$ , viscosity  $\eta=10~{\rm mPa}$  s, capillary length  $a=1.53~{\rm mm}$  and radius R between 0.8 and 2.0 mm) are released a few centimeters above a still liquid nitrogen bath, using calibrated needles. Liquid nitrogen, with density  $\rho_{\rm N}=808~{\rm kg~m}^{-3}$  is kept in a beaker with a diameter of 10 cm, and insulated (using a sacrificial bath²) to keep it from boiling. Due to the large temperature gradient between the drops (initially at ambient temperature) and the bath (at its boiling temperature,  $-196~{\rm ^{\circ}C}$ ) nitrogen evaporates rapidly below the drops. The nitrogen flow maintains drops in levitation, in an "inverse Leidenfrost" state.  $^{1,2,25,26}$  In the absence of direct contact with the liquid surface that sustains them and at the small velocities V considered here ( $V<10~{\rm cm~s}^{-1}$ ) the droplets motion is only limited by friction forces arising from

Paper Soft Matter

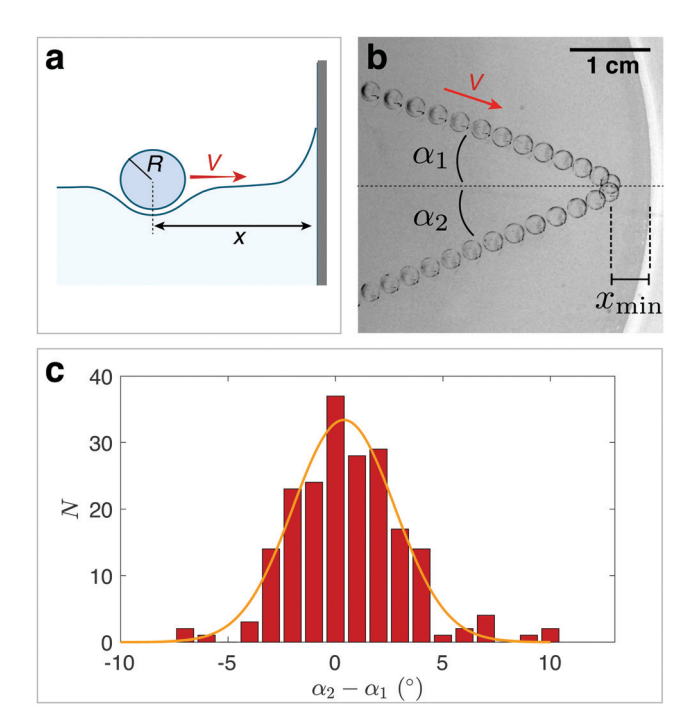


Fig. 1 (a) A silicone oil drop, with radius R is maintained in levitation above a liquid nitrogen bath. It hovers without effective friction: we consider its motion and dynamics as it approaches a wall. (b) Top view of an experiment. A drop with radius R = 1.2 mm is repelled by the wetting meniscus against a wall. We name  $\alpha_1$  the angle of incidence,  $\alpha_2$  the reflected angle and  $x_{\min}$  the minimum distance between the center of the droplet and the wall. See also ESI,† Movie 1. (c) Difference  $\alpha_2 - \alpha_1$ measured for more 200 rebounds, with 0.5° <  $\alpha_1$  < 30°. The drops are almost always perfectly reflected, with  $|\alpha_2 - \alpha_1| < 5^\circ$ . The orange line is a Gaussian fit, with standard deviation  $\sigma = 2.4^{\circ}$ 

shear within the vapor film. 4,8,26 Dissipation is thus extremely low: the residual skin friction is more than ten times smaller than the usual Stokes drag (in wetting situations) or the wave resistance drag (appearing at higher velocities).7 In addition, a self-propulsion mechanism almost perfectly compensates the remaining friction. Here, contrary to what is seen on solid surfaces,<sup>5</sup> self-propulsion is not linked to the internal motion of the droplet (which rapidly freezes), but arises from a spontaneous symmetry breaking within the film below the drop.<sup>26</sup> Vapor is then partially redirected and drags the drop along with it. Quickly after deposition, friction and propulsion compensate and the effectively frictionless drops move in straight lines (at a constant velocity V) along a direction randomly set by the initial symmetry breaking. The droplets deform the surface of the bath by their weight, generating a local depression of the interface, as illustrated in Fig. 1a. We consider the interaction of an incoming droplet (with radius R and velocity V) with a wall. Experiments are optically recorded from the top, using a high speed camera (Photron Mini UX-100) at a typical framerate of 500 fps, and the drops are tracked using an in-house Python algorithm.

Fig. 1b and ESI,† Movie 1 present a top-view recording of a typical bouncing experiment, with an interframe time of 60 ms. A drop (with radius R = 1.2 mm) approaches the glass wall of the beaker (in white) and is repelled from it. The particle has an

initial velocity  $V = 3.5 \pm 0.1 \text{ cm s}^{-1}$  (indicated with a red arrow) and approaches the wall with an initial angle  $\alpha_1$  = 20.0  $\pm$ 0.5 degrees measured with respect to the normal to the wall. From Fig. 1b one can infer that the rebound is close to a perfect reflection, with a reflected angle  $\alpha_2$  = 21.5  $\pm$  0.5 degrees. By measuring the difference between the incoming and reflected angles  $\alpha_2$ - $\alpha_1$  for more than 200 bouncing events (with  $\alpha_1$  varying between 0.5 and 30°), we show in Fig. 1c that this is a general feature of our system. The orange line is the best Gaussian fit to the experimental data, with a standard deviation  $\sigma = 2.4^{\circ}$ . In addition, Fig. 1b shows that during the rebound, the drops do not come in contact with the wall but come to a stop at a distance  $x = x_{\min}$  from it before bouncing back. In Fig. 1b,  $x_{\rm min}$  = 3.5  $\pm$  0.1 mm, a distance that is of the order of the diameter of the incoming object.

## 2 Wall rebounds

#### Capillary interaction

We interpret these results as a consequence of the meniscus repellency, Liquid nitrogen, with surface tension  $\gamma = 8.85 \, 10^{-3} \, \text{N m}^{-1}$ rises along the glass wall and generates a wetting meniscus (Fig. 1a). Locally, the shape of the liquid surface h(x) (with x the distance to the wall) is determined by an equilibrium between the pressure change across the interface due to surface tension, and the hydrostatic pressure difference due to the rise of the liquid. This is expressed by the Young-Laplace equation:

$$\frac{\mathrm{d}^2 h}{\mathrm{d}x^2} \left[ 1 + \left( \frac{\mathrm{d}h}{\mathrm{d}x} \right)^2 \right]^{-3/2} = \frac{\rho_{\mathrm{N}}gh}{\gamma} = \frac{h}{a^2} \tag{1}$$

where g stands for gravity,  $\rho_N$  for the density of liquid nitrogen and  $a = \sqrt{\gamma/\rho_{\rm N}g} = 11$  mm is the capillary length of liquid nitrogen. This equation has the analytic solution: 27,28

$$x - x_0 = a \operatorname{acosh}\left(\frac{2a}{h}\right) - 2a\left(1 - \frac{h^2}{4a^2}\right)^{1/2}$$
 (2)

with  $x_0$  an integration constant, chosen so that  $h(x = x_0) = h^*$ where  $h^*$  equals the height of the meniscus at the wall. For small deformations (in particular, far enough from the wall),

eqn (1) can be simplified to 
$$\frac{d^2h}{dx^2} = \frac{h}{a^2}$$
, which yields:

$$h(x) = a \cot \beta \exp^{-x/a}.$$
 (3)

Here,  $\beta$  is a constant that can be seen as an extrapolated contact angle, obtained by matching the small slope approximation close to the wall. However, the small slope approximation does not necessarily hold close to the wall, especially for wetting liquids, and the value of  $\beta$  is expected to overestimate the apparent (macroscopic) contact angle  $\theta$ , as we will see later.

When a particle approaches the wall, interaction between the depression of the interface around the drop and the wetting meniscus at the wall induces a capillary interaction potential E<sub>c</sub>, which, following Vella and Mahadevan, <sup>19</sup> we estimate as the product of the effective weight of the particle W with the meniscus shape h(x). For perfectly non-wetting particles ( $\theta = 180^{\circ}$ ),

Soft Matter Paper

W simplifies to  $W = mg \frac{\rho}{\rho_N}$  with m the drop mass, so that:

$$E_{\rm c}(x) = mg \frac{\rho}{\rho_{\rm N}} h(x). \tag{4}$$

Note that  $E_c(x) > 0$  here, which indicates repellency.

### **Bouncing dynamics**

In our experiment, and contrary to other non-wetting situations without self-propulsion24 the droplets are effectively frictionless: the kinetic energy of an approaching droplet  $E_k = \frac{1}{2}mV^2$  is simply converted into potential energy as it climbs the liquid slide. The particle turns back when its velocity perpendicular to the wall is zero, at a position  $x = x_{\min}$  (as seen in Fig. 1b). Energy conservation between the positions  $x = +\infty$  and  $x = x_{min}$  simply implies  $\frac{1}{2}mV_x^2 = mg\frac{\rho}{\rho_N}h(x_{\min})$ , with  $V_x$  the initial velocity of the particule normal to the wall. Using eqn (2), this gives the expression of  $x_{\min}$ :

$$x_{\min} = x_0 + a \operatorname{acosh}\left(\frac{2a}{h_{\min}}\right) - 2a\left(1 - \frac{h_{\min}^2}{4a^2}\right)^{1/2}$$
 (5)

with  $h_{\rm min}=rac{V_x^2}{2g}\left(rac{
ho}{
ho_{
m N}}
ight)$  the height for which all the initial kinetic energy of the droplet is converted into potential energy.

In Fig. 2a, we report the experimental measurements of  $x_{\min}$ as a function of the initial drop velocity  $V_x$  normal to the wall. As predicted by eqn (5),  $x_{\min}$  does not depend on the drop size, and the data obtained for varying R (0.8 mm < R < 2 mm) overlap. The solid black line shows eqn (5), which matches the experimental data, with a fitting parameter  $x_0 = 0.45$  mm. By reporting  $x_0$  in eqn (2), one can extrapolate the meniscus profile from  $x = x_{\min}$  up to the wall (x = 0) and estimate the apparent (macroscopic) contact angle. Using  $tan(\theta_{app}) = \left(\frac{dx}{dh}\right)_{x=0}$ , we

obtain  $\theta_{\rm app} \simeq 30^{\circ}$ . Even if liquid nitrogen is perfectly wetting (with a surface tension  $\gamma = 8.85$  mN m<sup>-1</sup>), the non-zero value of  $\theta_{app}$  is consistent with an apparent (evaporative) contact angle, which value is set by the local heat fluxes at the wall.<sup>29-32</sup> The validity of our extrapolation of the meniscus shape, in a situation far from equilibrium as here, will need further experimental and theoretical confirmation.

Fig. 2 also shows that in the region reached by the droplets  $(x \ge 1.5 \text{ mm})$ , the small-slope approximation (indicated by a large gray line) perfectly overlaps the exact solution of the Young-Laplace equation, with a fitting parameter  $\beta = 50^{\circ}$ . Eqn (3) underestimates the meniscus deformation, and thus overestimates the apparent contact angle, which explains why  $\beta > \theta_{\rm exp}$ . In the following, we will thus consider  $\beta$  as a fitting parameter.

The capillary interaction model is further confirmed by following the center of mass of the particles as they bounce off the wall. In Fig. 2b, we plot the velocity V of two drops with sizes R = 1.4 mm (blue dots) and R = 0.8 mm (red dots) as a function of time t. The velocities before and after impact are nearly identical and the rebound itself (which lasts typically 200 ms) is perfectly elastic, indicating that there is indeed no effective friction here. The two droplets have different impact angles ( $\alpha_1 = 12^{\circ}$  for R = 1.4 mm and  $\alpha_1 = 1^{\circ}$  for R = 0.8 mm). As visible in Fig. 2b, this marginally impacts the velocity profile V(t), which decreases to  $V_{\min} \simeq 1 \text{ cm s}^{-1}$  for  $\alpha_1 = 12^{\circ}$ , while  $V_{\rm min} \simeq 0$  for  $\alpha_1 = 1^{\circ}$ . Using eqn (3) and (4), we integrated the equations of motion of the two droplets, and plotted the resulting velocities V(t) as a slightly darker line on top of the experimental data of Fig. 2b. The model nicely matches the experiments, indicating that the droplets dynamics can be fully modelled with a single repulsive capillary force  $\vec{F} = -dE_c/dx \ \vec{e}_x$ .  $\vec{F}$  is normal to the wall, which also explains why the rebounds are close to perfect reflections, as seen in Fig. 1c.

These results show that in absence of friction, non-wetting droplets behave as capillary probes: one can infer from their

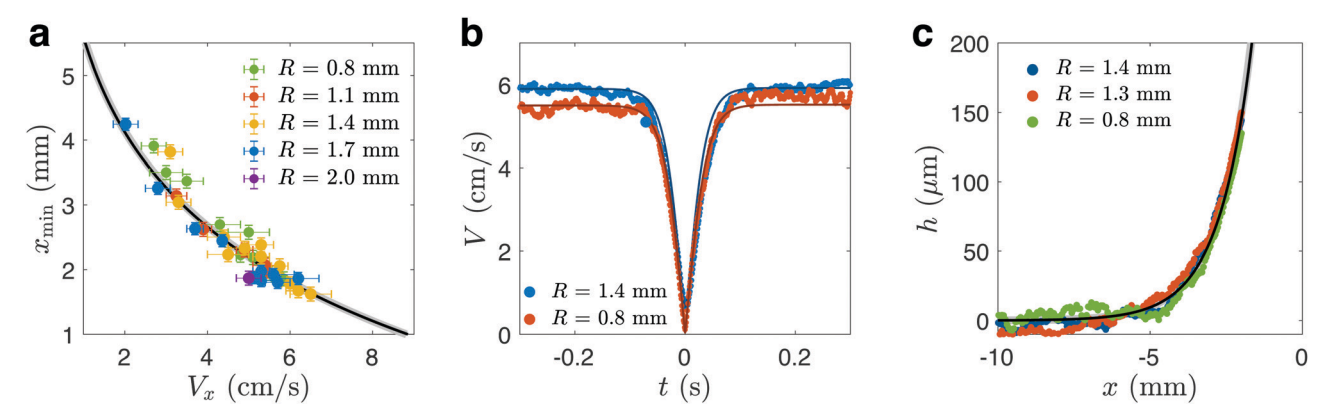


Fig. 2 (a) Minimal distance  $x_{min}$  between the drop center and the wall for multiple bouncing events, as a function of its incoming velocity  $V_x$  and for varying drop sizes (0.8 mm < R < 2 mm). The black line is the theoretical plot, from eqn (2) and with a constant  $x_0 = 0.45$  mm. The larger gray line is the small-slope approximation from eqn (3), with  $\beta = 50^{\circ}$ . (b) Particle velocity V as a function of time t at it is repelled by the wall. The blue and red dots (respectively for R = 1.4 mm,  $\alpha_1 = 12^\circ$  and R = 0.8 mm,  $\alpha_1 = 1^\circ$ ) are experiments, and the lines show the model. (c) Comparison between the theoretical meniscus shape h(x) (in black, eqn (2) with fitting parameter  $x_0 = 0.45$  mm and in gray, eqn (3), with  $\beta = 50^{\circ}$ ) and the shape reconstructed from the droplet dynamics (colored dots) for three different drop radii.

Soft Matter **Paper** 

dynamics any meniscus shape h(x) through the capillary interaction potential in the region reached by the droplets. We demonstrate this in Fig. 2c, where we compare the

meniscus height calculated from the droplet dynamics h(x) =

$$\frac{1}{2g} \left( \frac{\rho_{\text{N}}}{\rho} \right) \left( V^2(x = \infty) - V^2(x) \right)$$
 to its theoretical value (in black).

The plots obtained for three different drop sizes are presented: they all overlap with the theoretical shape h(x), demonstrating that the droplets indeed behave as interfacial probes. In Fig. 2c, the analytic solution of the Young-Laplace equation (in black, eqn (2)) and the small slope approximation (in gray, eqn (3)) overlap, with the same fitting parameters as in Fig. 2a:  $x_0 = 0.45 \text{ mm} \text{ and } \beta = 50^{\circ}.$ 

## 3 Drop manipulation

In the following, we aim at directing the drop motion by using the menisci of well-defined wall geometries. We illustrate this with two examples: a droplet gun created by means of confinement within a channel and droplet focusing using parabolic walls.

#### Channels

In Fig. 3a, a drop (of radius R = 0.9 mm) is deposited inside a narrow channel (with width d = 3 mm, length 6.5 cm and height 1.5 cm). The channel walls are partially immersed into the bath, and they rise approximately one centimeter above the liquid nitrogen surface. The orange line depicts the drop trajectory after its deposition. Due a spontaneous symmetry breaking within the vapor film that sustains it, the drop is initially selfpropelled within the channel in a random direction. It is then

repelled by both walls and bounces back and forth a large number of times before the very small dissipation experienced by the drop stabilizes it in the center of the gutter formed by the meniscus. The drop is thereby forced to slide in the direction of the channel, at a constant velocity fixed by the equilibrium between propulsion and friction. As visible in Fig. 3a and ESI,† Movie 2, the particle maintains the enforced direction for several centimeters after escaping the channel. Fig. 3b shows the superposition of twenty drop trajectories before and after escaping two channels with width d = 3 mm and d = 6 mm. When the channel size and the drop size are comparable (top image) the drops are almost perfectly guided: the spreading angle (measured at the exit of the channel) equals 1.6°. The same drop deposited in a wider channel, however, will still be guided but less efficiently: for d = 6 mm, the spreading angle reaches 30 degrees (Fig. 3b, bottom image).

Interestingly, the channels do not only guide the drops, but also accelerate them in a controlled and reproducible manner. Fig. 3c shows the drop velocities V inside (x < 0) and outside (x > 0) the channel for ten identical experiments. Inside the channel, the drop velocities  $V_i$  are on the order of 3 cm s<sup>-1</sup>, but V is multiplied by almost a factor 3 when the drops escapes with  $V_{\rm f} \simeq 8.5~{\rm cm~s^{-1}}$ . In our experiment, the velocity  $V_{\rm f}$  is higher than the terminal velocity ( $v_0 \simeq 5 \text{ cm s}^{-1}$ ) of the self-propelled droplets and friction causes a slow deceleration visible for x > 1 cm. In Fig. 3d, we report the non-dimensional variation of the kinetic energy of the drop  $\Delta V^2/2ga$  with  $\Delta V^2 = V_f^2 - V_i^2$  for varying channel widths d (3 mm < d < 10 mm, black dots), and drop sizes (0.7 mm < R < 1.3 mm, in blue). As the channel size increases, the drops are less and less accelerated until nothing happens for d/a > 10. In addition, the data obtained for varying drop radii almost perfectly overlap in Fig. 3d,

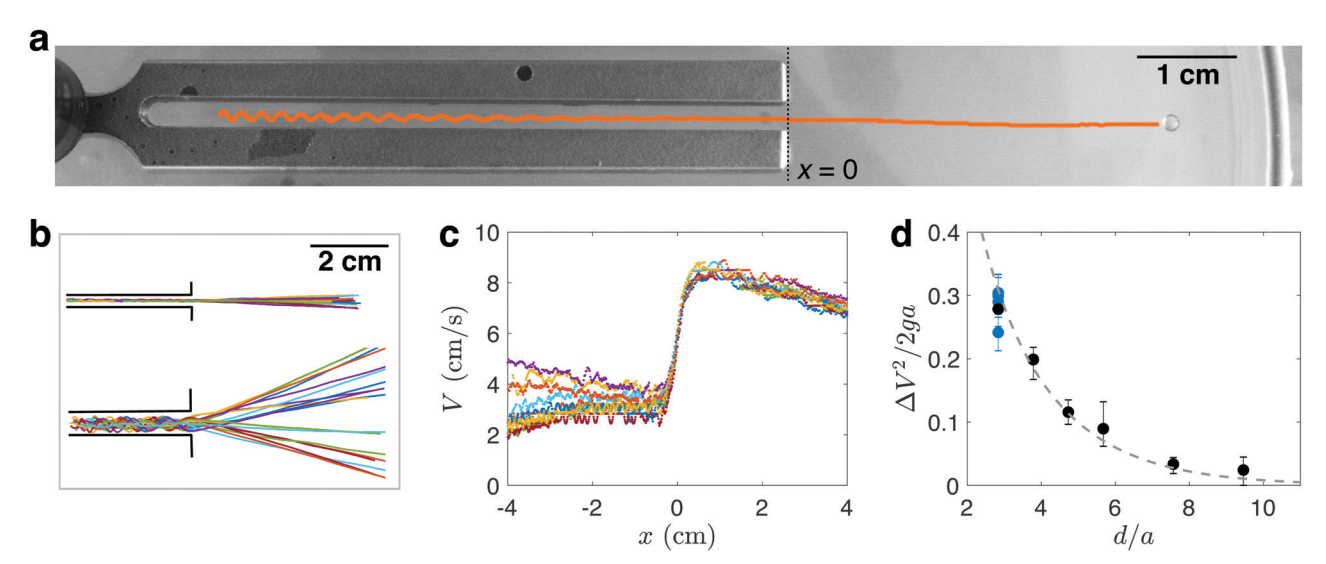


Fig. 3 (a) Top view of a droplet gun experiment. A silicone oil drop with radius  $R = 900 \, \mu \text{m}$  is deposited into an aluminium channel (with size  $d = 3 \, \text{mm}$ ) semi-immersed in the bath. Its trajectory is plotted in orange. After a few bounces against the walls, the drop is directed along the channel. See also ESI,† Movie 2. (b) Trajectories of 20 drops (with radius  $R = 900 \mu m$ ) emerging from two channels, with d = 3 mm (top) and d = 6 mm (bottom). (c) Velocity Vinside (x < 0) and out (x > 0) of a channel with width d = 3 mm, for 10 droplets of radius R = 900  $\mu$ m. The drops slide along the meniscus and their velocity is more than doubled when they escape. (d) Non-dimensional increase of the droplet kinetic energy, for varying channel size d between 3 and 10 mm (black points) and drop radii R between 0.8 mm and 1.4 mm (in blue). The dotted line is the theoretical model.

Soft Matter

indicating that the strength of the acceleration does not depend on the drop size.

What causes the acceleration? The distance d between the walls is comparable to the capillary length, allowing the two menisci on each side to interact with each other, inducing a capillary rise in the channel. The height H of liquid nitrogen inside of the channel is then simply determined by a 2D Jurin's law, and only depends on the distance d between the two walls and on the apparent contact angle at the wall. To simplify, we use the small-slope approximation of Young-Laplace equation, which, as demonstrated before, matches well the shape of the meniscus felt by the droplets. Integration then gives:

$$H = 2a \cot \beta \left( \frac{\cosh(d/2a)}{\sinh(d/a)} \right). \tag{6}$$

For d = 3 mm and  $\beta = 50^{\circ}$ ,  $H \sim 250 \,\mu\text{m}$ , which is smaller, but on the order of magnitude of the drop size. When a particle deposited inside the channel reaches the edge, it slides down the liquid slope to reach the bath level. In the process, its potential energy is converted into kinetic energy so that  $1/2m(V_f^2 - V_i^2) = mgH$ . For  $H = 250 \ \mu m$  and  $V_i = 3 \ cm \ s^{-1}$ , we expect  $V_{\rm f}$  to reach 7.5 cm s<sup>-1</sup>, which is close to the velocity out of the channel measured in Fig. 3b. Using eqn (6), we can thus predict the increase of the particles kinetic energy as they slide down the slope. In non-dimensional form, we find:

$$\frac{\Delta V^2}{2ga} = 2\cot\beta \left(\frac{\cosh(d/2a)}{\sinh(d/a)}\right) \tag{7}$$

Eqn (7) is reported in Fig. 3d as a dotted line, which is found to nicely match the experimental data, with a fitting parameter  $\beta = 62^{\circ}$ . This value is slightly higher than what was found for the bouncing on a single glass wall (Section 2): here the channels are made of aluminum, a conductive metal, which enhances evaporation at the meniscus and might thus increase the extrapolated small-slope contact angle  $\beta$ .

## **Drop focusing**

These channels can be used in combination with other tools to finely control drop motion. We show an example of it in Fig. 4 and ESI,† Movie 3, where we use both a channel and a parabolic wall to focus drops in a specific location. This parabolic "mirror" is visible on the right in Fig. 4a and it is designed with a focal length of 5 cm. Using a 3 mm wide channel, drops are launched parallel to the axis of the mirror and their trajectories are tracked before and after bouncing. The trajectory of a drop with radius  $R = 830 \mu m$  is shown in blue in Fig. 4a and a blue arrow indicates its initial direction of motion. The drop is reflected by the wall and exhibits a trajectory quite similar to what might be expected of light reflected on a parabolic mirror. To verify this, we repeated the same experiment multiple times by changing the position of the channel with respect to the focal axis of the parabola. The corresponding drop trajectories are represented in Fig. 4b. The continuous lines are the experimental trajectories (measured as soon as the drops leave the channel) and the dotted lines are linear extrapolations before and after the rebound. On Fig. 4b,

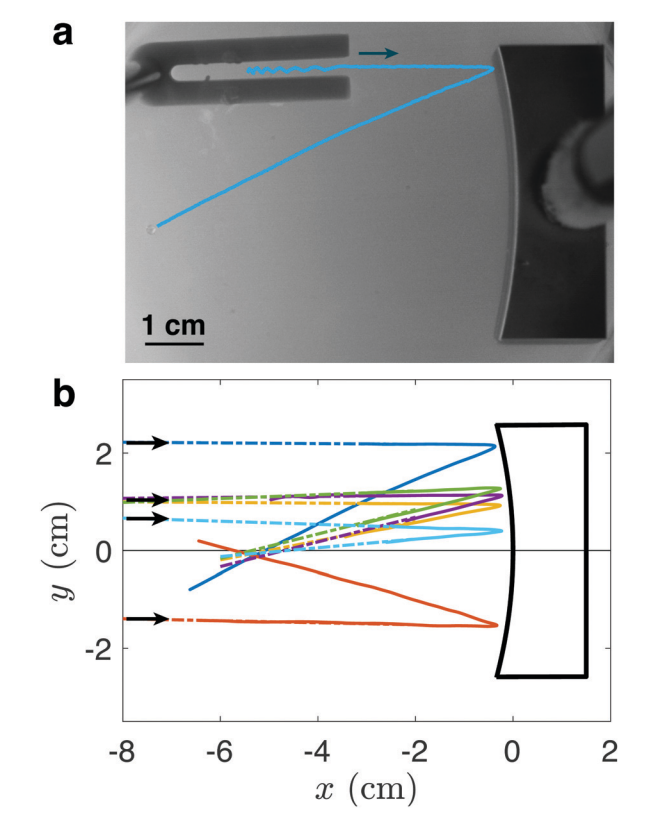


Fig. 4 (a) Top view of the trajectory of a drop (radius  $R = 830 \mu m$ ) directed towards a parabolic mirror (with focal length 5 cm). See also ESI,† Movie 3. (b) Trajectories of 6 drops, initially parallel to the axis of the mirror. They are all deflected towards the focal point.

all drop trajectories cross the principal axis of the parabolic mirror at position  $x = 5.4 \pm 0.3$  cm, a value that is very close to the actual focal length, efficiently gathering the droplets at this specific location. This experiment is similar in spirit to the deflection of gliding droplets by a cylinder, which was discussed recently by Hale and Boudreau.<sup>24</sup> By using a concave object instead of a convex one, droplets are scattered on the liquid surface instead of being focused, which is another nice demonstration of how capillary forces can be harnessed to direct drops.

## 4 Conclusion

By studying the collision dynamics of a droplet with a meniscus on a single wall, we show that frictionless particles are a good tool to probe interfaces. The surface deformation can be directly inferred from the variation of the particle's kinetic energy (in any region reached by the droplet), which we demonstrate by reconstructing the meniscus shape up to 1.5 mm from the wall. By extrapolating the section of the meniscus probed by the droplets, we can get a first estimate of the apparent contact angle of liquid nitrogen at the wall, which is dominated by the evaporation process rather than by an equilibrium of surface tension forces only. A more specific study is however necessary to validate the extrapolation of the meniscus shape in such a non-equilibrium situation.

Paper Soft Matter

In a second part, we show that, counter-intuitively, it is easier to control drops on a liquid bath than on solids. The menisci efficiently repel drops with extremely low energy loss (for our Leidenfrost droplets) and cause almost perfect reflections. In addition, drop "waveguides" can be made by placing them between two walls. By tuning the distance between the walls, one can choose the strength of the acceleration that the drops undergo upon escape. To push this further, one could combine simple geometrical elements into more complex setups that could handle multiple drops at the same time and select, sort them and mix them.

## Conflicts of interest

The authors declare no conflict of interest.

## Notes and references

- 1 Y. S. Song, D. Adler, F. Xu, E. Kayaalp, A. Nureddin, R. M. Anchan, R. L. Maas and U. Demirci, Proc. Natl. Acad. Sci. U. S. A., 2010, 107, 4596-4600.
- 2 M. Adda-Bedia, S. Kumar, F. Lechenault, S. Moulinet, M. Schillaci and D. Vella, Langmuir, 2016, 32, 4179-4188.
- 3 J. G. Leidenfrost, De aquae communis nonnullis qualitatibus tractatus, Ovenius, 1756.
- 4 A.-L. Biance, C. Clanet and D. Quéré, Phys. Fluids, 2003, 15, 1632-1637.
- 5 A. Bouillant, T. Mouterde, P. Bourrianne, A. Lagarde, C. Clanet and D. Quéré, Nat. Phys., 2018, 14, 1188-1192.
- 6 S. Lyu, V. Mathai, Y. Wang, B. Sobac, P. Colinet, D. Lohse and C. Sun, Sci. Adv., 2019, 5, eaav8081.
- 7 M. Le Merrer, C. Clanet, D. Quéré, É. Raphaël and F. Chevy, Proc. Natl. Acad. Sci. U. S. A., 2011, 108, 15064-15068.
- 8 J. Hale and C. Akers, J. Fluid Mech., 2016, 803, 313-331.
- 9 L. Maquet, B. Sobac, B. Darbois-Texier, A. Duchesne, M. Brandenbourger, A. Rednikov, P. Colinet and S. Dorbolo, Phys. Rev. Fluids, 2016, 1, 053902.
- 10 X. Ma, J.-J. Liétor-Santos and J. C. Burton, Phys. Rev. Fluids, 2017, 2, 031602.

- 11 H. Linke, B. Alemán, L. Melling, M. Taormina, M. Francis, C. Dow-Hygelund, V. Narayanan, R. Taylor and A. Stout, Phys. Rev. Lett., 2006, 96, 154502.
- 12 T. R. Cousins, R. E. Goldstein, J. W. Jaworski and A. I. Pesci, I. Fluid Mech., 2012, 696, 215-227.
- 13 M. M. Nicolson, Proc. Cambridge Philos. Soc., 1949, 288.
- 14 P. Peruzzo, A. Defina, H. M. Nepf and R. Stocker, Phys. Rev. Lett., 2013, 111, 164501.
- 15 M. Cavallaro, L. Botto, E. P. Lewandowski, M. Wang and K. J. Stebe, Proc. Natl. Acad. Sci. U. S. A., 2011, 108, 20923-20928.
- 16 D. Ershov, J. Sprakel, J. Appel, M. A. C. Stuart and J. van der Gucht, Proc. Natl. Acad. Sci. U. S. A., 2013, 110, 9220-9224.
- 17 E. Bormashenko, Y. Bormashenko, R. Grynyov, H. Aharoni, G. Whyman and B. P. Binks, J. Phys. Chem. C, 2015, 119, 9910-9915.
- 18 C. H. Ooi, A. Van Nguyen, G. M. Evans, O. Gendelman, E. Bormashenko and N.-T. Nguyen, RSC Adv., 2015, 5, 101006-101012.
- 19 D. Vella and L. Mahadevan, Am. J. Phys., 2005, 73, 817-825.
- 20 D. L. Hu and J. W. Bush, Nature, 2005, 437, 733.
- 21 J.-L. Liu, X.-Q. Feng and G.-F. Wang, Phys. Rev. E: Stat., Nonlinear, Soft Matter Phys., 2007, 76, 066103.
- 22 Y. Su, B. Ji, Y. Huang and K.-C. Hwang, Langmuir, 2010, 26, 18926-18937.
- 23 T. Darmanin and F. Guittard, Mater. Today, 2015, 18, 273-285.
- 24 J. Hale and J. Boudreau, Phys. Rev. Fluids, 2019, 4, 033602.
- 25 H. Feng, Y. Xu and T. Yang, Int. J. Heat Mass Transfer, 2018, 127, 413-421.
- 26 A. Gauthier, C. Diddens, R. Proville, D. Lohse and D. van der Meer, Proc. Natl. Acad. Sci. U. S. A., 2019, 116, 1174-1179.
- 27 L. Landau and E. Lifshitz, Theoretical Physics, Fluid Mechanics, 1987, vol. 6.
- 28 P.-G. De Gennes, F. Brochard-Wyart and D. Quéré, Capillarity and wetting phenomena: drops, bubbles, pearls, waves, Springer Science & Business Media, 2013.
- 29 S. Morris, J. Fluid Mech., 2001, 432, 1-30.
- 30 G. Berteloot, C.-T. Pham, A. Daerr, F. Lequeux and L. Limat, EPL, 2008, 83, 14003.
- 31 A. Y. Rednikov and P. Colinet, Microgravity Sci. Technol., 2010, 22, 249-255.
- 32 V. Janeček and V. Nikolayev, EPL, 2012, 100, 14003.